

## Homoclinic snaking in bounded domains

S. M. Houghton<sup>1,\*</sup> and E. Knobloch<sup>2,†</sup><sup>1</sup>*School of Mathematics, University of Leeds, Leeds LS2 9JT, United Kingdom*<sup>2</sup>*Department of Physics, University of California, Berkeley, California 94720, USA*

(Received 27 February 2009; revised manuscript received 27 May 2009; published 20 August 2009)

Homoclinic snaking is a term used to describe the back and forth oscillation of a branch of time-independent spatially localized states in a bistable spatially reversible system as the localized structure grows in length by repeatedly adding rolls on either side. On the real line this process continues forever. In finite domains snaking terminates once the domain is filled but the details of how this occurs depend critically on the choice of boundary conditions. With periodic boundary conditions the snaking branches terminate on a branch of spatially periodic states. However, with non-Neumann boundary conditions they turn continuously into a large amplitude filling state that replaces the periodic state. This behavior, shown here in detail for the Swift-Hohenberg equation, explains the phenomenon of “snaking without bistability,” recently observed in simulations of binary fluid convection by Mercader *et al.* Phys. Rev. E **80**, 025201 (2009).

DOI: 10.1103/PhysRevE.80.026210

PACS number(s): 47.54.-r, 47.20.Ky

### I. INTRODUCTION

Recent years have seen rapid developments in the theory of spatially localized structures in reversible systems in both one [1–3] and two [4–6] spatial dimensions. These structures occur in a great variety of physical systems, including nonlinear optics where they are usually referred to as dissipative solitons, reaction-diffusion systems where they take the form of spots or ensembles of spots, and convection where they are called convectons. We refer to a recent special issue of *Chaos* [7] for an overview of the subject, including applications, and to [8] for a discussion of open problems in this area.

The theory is simplest in one spatial dimension and relies on the presence of bistability between a trivial state and a spatially periodic state: on the real line spatially localized states first appear via a bifurcation from the trivial state and do so simultaneously with the primary branch of spatially periodic states. Typically there are two branches of spatially localized states that are produced, both symmetric under reflection  $x \rightarrow -x$ , with either maxima or minima at  $x=0$ . In the following we refer to these states in terms of their spatial phase  $\phi=0, \pi$  as  $L_{0,\pi}$ , respectively. These states are distinct and are not related by symmetry. Both  $L_{0,\pi}$  bifurcate in the same direction as the periodic states, i.e., subcritically, and are initially unstable. With decreasing parameter the localized states grow in amplitude but shrink in extent; when the extent of the localized state approaches one wavelength and the amplitude reaches that of the competing periodic state the branch enters the so-called snaking or pinning region and begins to “snake” back and forth. As this happens the localized state gradually adds rolls, symmetrically on either side, thereby increasing its length. As a result the localized states high up the snaking branches resemble the finite amplitude spatially periodic state over longer and longer lengths. Typically each snaking branch repeatedly gains and loses stability

via saddle-node bifurcations, producing an infinite multiplicity of coexisting stable states within the pinning region. Secondary bifurcations to pairs of (unstable) branches of asymmetric states are found in the vicinity of each saddle node; these branches resemble “rungs” that connect the two snaking branches and are responsible for the “snakes-and-ladders” structure of the pinning region [1,4]. The origin and properties of this behavior are now quite well understood, at least in variational systems [2,3,9,10]. However, in addition to these states there are spatially localized states that resemble “holes” in a background of otherwise spatially peri-

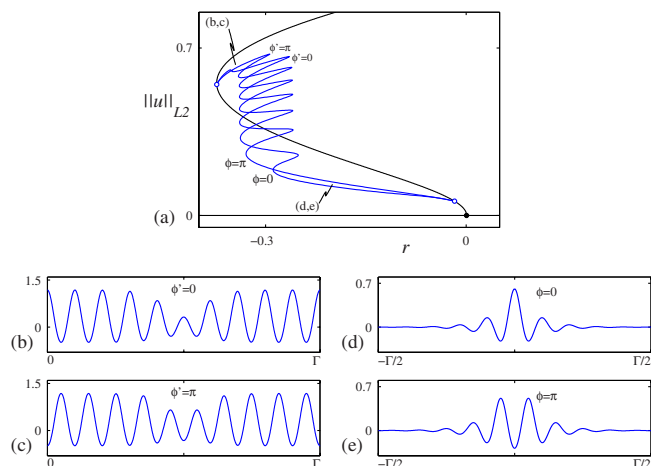


FIG. 1. (Color online) (a) Bifurcation diagram showing the equivalent of homoclinic snaking in the Swift-Hohenberg equation with  $b_2=1.8$  on a periodic domain with period  $\Gamma=62$ . The snaking branches  $L_0$  and  $L_\pi$  emerge from  $P_{10}$  in a secondary bifurcation ( $\odot$ ) at small amplitude and terminate on the same branch in a secondary bifurcation ( $\odot$ ) near the saddle node. Other spatially periodic branches are also present but for clarity are not shown. [(b) and (c)] Sample profiles from the  $\phi'=0$  and  $\phi'=\pi$  branches near the upper end of the snaking branches. [(d) and (e)] Sample profiles from the  $\phi=0$  and  $\phi=\pi$  branches on the lower part of the snaking branches. In this case the  $L_0$  branch connects the  $\phi=0$  and  $\phi'=0$  solutions, and the  $L_\pi$  branch connects the  $\phi=\pi$  and  $\phi'=\pi$  solutions. After [12].

\*smh@maths.leeds.ac.uk

†knobloch@berkeley.edu

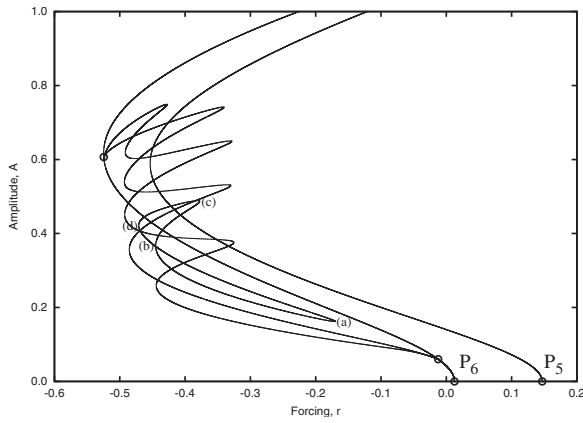


FIG. 2. Bifurcation diagram showing the equivalent of homoclinic snaking with Neumann boundary conditions on a domain of length  $2L=40$ . Only even-parity states are shown. Pitchfork bifurcations are denoted by  $\circ$ . Solution profiles  $u(x)$  at the saddle nodes (a)–(d) are shown in Fig. 4.

odic finite amplitude wave trains [11]. These bifurcate from the vicinity of the saddle-node bifurcation on the branch of spatially periodic states and are also organized into a pair of branches with its own snakes-and-ladders structure produced as the hole deepens and fills with longer and longer sections of the trivial state.

On an unbounded domain these two pairs of snaking branches remain distinct. This is not so, however, once the domain becomes finite [12]. In this case neither set of branches can snake forever, and the snaking process must terminate when the width of the localized periodic state approaches the domain size and likewise for the width of the localized hole. Thus both pairs of branches must turn over and exit the snaking region. Typically the two pairs of branches connect pairwise (Fig. 1) so that the small amplitude  $\phi=0$  branch now connects to the corresponding branch of holelike states and likewise for the  $\phi=\pi$  branch. This figure, computed for the quadratic-cubic Swift-Hohenberg equation on a periodic domain of period  $\Gamma=62$ , shows that the classic localized states enter the pinning region from small amplitude on the right and exit this region at large amplitude toward the left; however, the same figure can also be viewed as showing that the holelike states enter the snak-

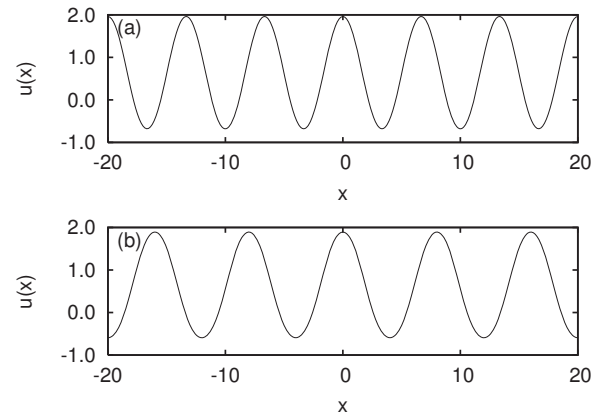


FIG. 3. Sample large amplitude periodic states  $u(x)$  on (a)  $P_6$  and (b)  $P_5$  with Neumann boundary conditions on a domain of length  $2L=40$ , both at  $r=0$ .

ing region at the top from the left and exit it near the bottom toward the right. One finds, in addition, that in domains of finite size, the branches of small amplitude localized states no longer bifurcate directly from the trivial state but now do so in a secondary (pitchfork) bifurcation on the primary branch of periodic states. The finite domain size likewise affects the bifurcation to the holelike states on the branch of periodic states: the two branches of holelike states need not bifurcate together and need not bifurcate from the primary periodic branch [12]. Thus, depending on the spatial period, the branches of spatially localized states may or may not terminate together on a branch of periodic states, and this branch may or may not be the branch from which these states bifurcate at small amplitude. However, despite these finite-size effects the behavior *within* the snaking region remains essentially identical to that present on the real line, with the effects of the finite size confined to the vicinity of the bifurcations creating the localized and holelike states in the first place [12]. Similar observations are made in Ref. [13] as well. Thus the physical interpretation of the structure of the snaking region in terms of front pinning [14] remains largely unchanged.

The above picture, attractive as it is, relies on the use of spatially periodic boundary conditions (PBCs) to approximate the real line. A recent study of binary fluid convection

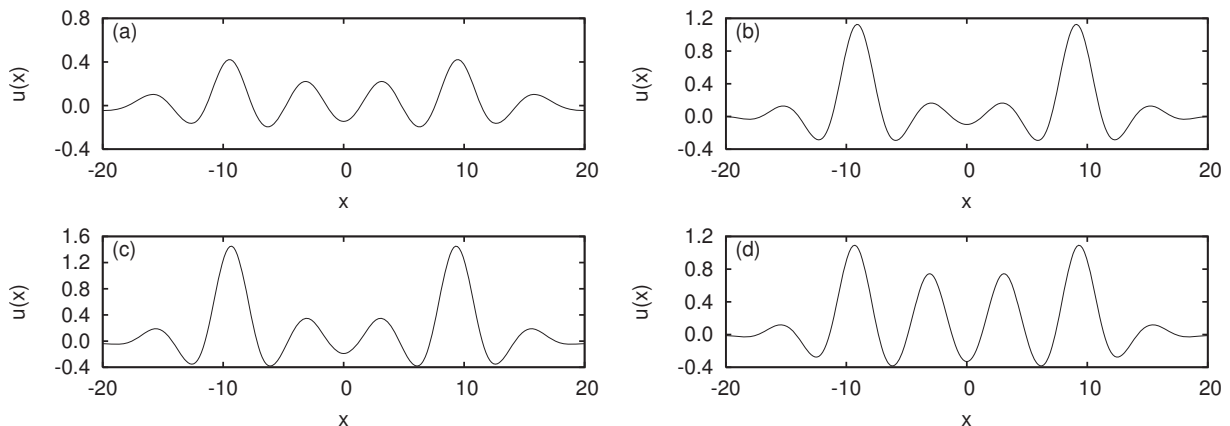


FIG. 4. Sample two-pulse profiles  $u(x)$  at the saddle nodes along the figure-eight isola in Fig. 2.

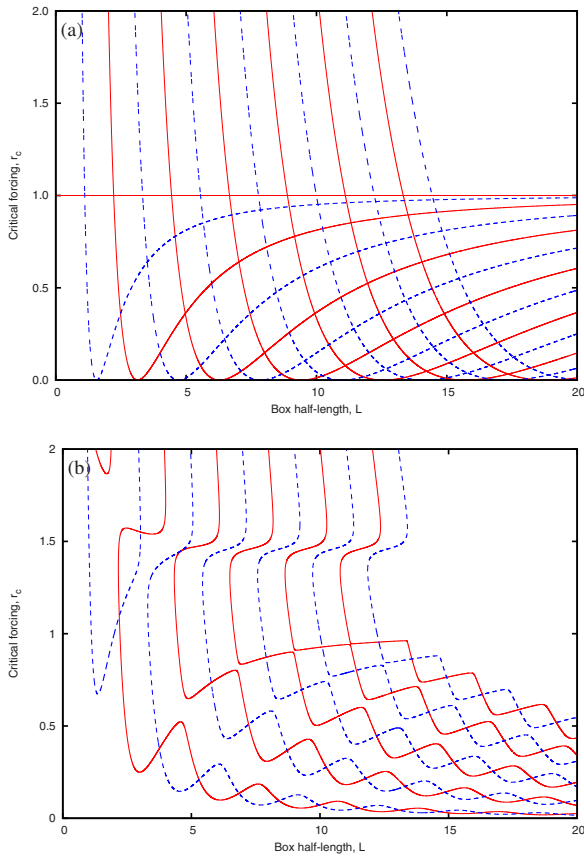


FIG. 5. (Color online) Neutral curves for (a)  $\beta=0$  and (b)  $\beta=0.5$  corresponding to even (red solid) and odd (blue dashed) eigenfunctions.

in a two-dimensional box with no-slip boundary conditions on all boundaries [15] reveals behavior that differs qualitatively from the above picture: the snaking branches do not terminate on a branch of periodic states that coexist with the conduction state and instead evolve continuously into large amplitude nonperiodic states that fill the box and play the role of the periodic state present with PBC. These states typically include a defectlike structure in order to accommodate the natural wavelength of the rolls, with additional de-

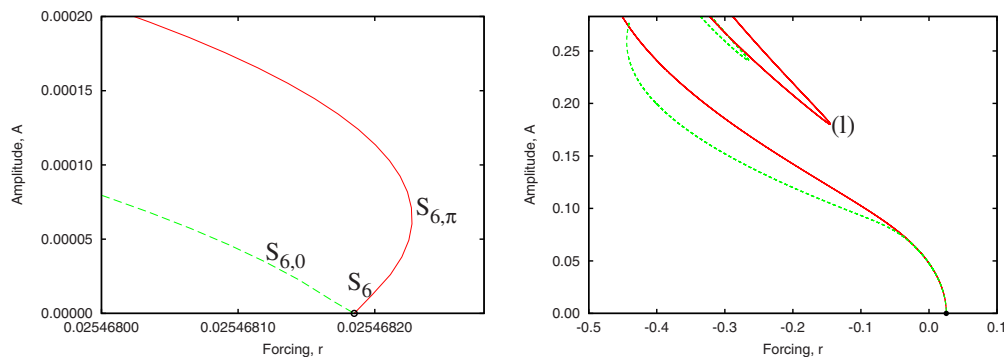


FIG. 7. (Color online) (a) With Robin boundary condition (2) the bifurcation at  $S_6$  becomes transcritical (solid dot): the  $\phi=\pi$  branch  $S_{6,\pi}$  now bifurcates supercritically but undergoes a saddle-node bifurcation close to threshold before turning toward negative values of  $r$ , while  $S_{6,0}$  bifurcates subcritically. Thus the breaking of the hidden reflection symmetry results in an apparent splitting of the  $P_6$  branch. (b) The same but on a larger scale, showing  $S_{6,0}$  (dashed green) and  $S_{6,\pi}$  (solid red) together with the two branches that become disconnected from them as a result of the broken hidden symmetry. Parameters:  $\beta=0.5$  and  $2L=40$ .

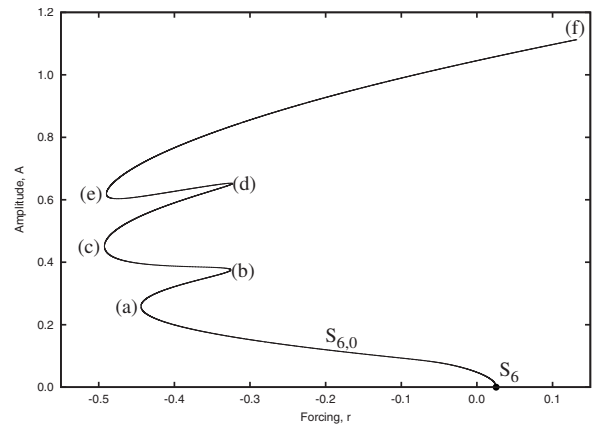


FIG. 6. Bifurcation diagram showing the equivalent of homoclinic snaking with Robin boundary conditions (2) and  $\beta=0.5$  on a domain of length  $2L=40$ . Only the  $\phi=0$  branch  $S_{6,0}$  is shown. Solution profiles  $u(x)$ , at the labeled points, are shown in Fig. 8.

fectlike structures present at either lateral boundary required by the no-slip boundary conditions. The authors of Ref. [15] refer to this situation as “snaking without bistability” since there is no large amplitude state that exists independently of the snaking branches.

We use these results to motivate our study in this paper of the Swift-Hohenberg equation with non-Neumann lateral boundary conditions. Neumann boundary conditions (NBCs) are special since problems with NBC on domains of length  $2L$  can be embedded in problems with PBC and period  $4L$  [16]. Thus the behavior described above for problems with PBC applies equally to problems with NBC. Consequently, we focus here on the effects of a generalization of Neumann boundary conditions referred to as Robin boundary conditions (RBCs). It should be emphasized that the change from Neumann to non-Neumann boundary conditions has a profound effect already on the linear stability problem. In the former case the null eigenfunctions (critical modes) are sinusoidal, with well-defined mode number  $n$ . The branches that bifurcate into the nonlinear regime preserve this mode number, and in the following we refer to them as  $P_n$ . Moreover, as  $L$  increases the neutral curves corresponding to

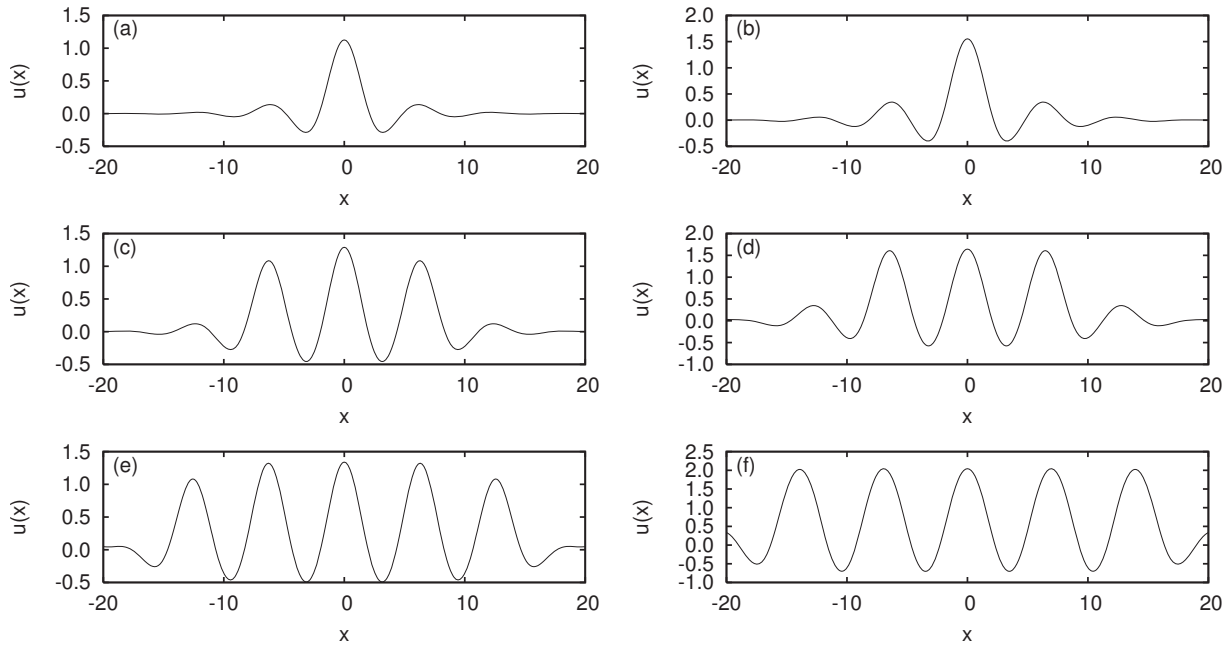


FIG. 8. Solution profiles  $u(x)$  at successive saddle nodes along the  $\phi=0$  branch  $S_{6,0}$  from small to large amplitude as indicated in Fig. 6. The final panel shows the  $\phi=0$  state at  $r=0.12997$ . Parameters:  $\beta=0.5$  and  $2L=40$ .

$n$  and  $n + 1$ , say, must cross; the corresponding codimension two points are key to understanding mode jumping in problems of this type, i.e., the transitions from one preferred wave number to another, in the nonlinear regime [17,18]. With non-Neumann boundary conditions, however, the situation is quite different. The neutral modes are either odd or even but have no well-defined wave number. It follows that when neutral curves corresponding to modes of like parity (odd-odd or even-even) cross, they generically reconnect [19], producing a quite different neutral curve topology. Only odd-even crossings remain structurally stable. Moreover, since the bifurcating solutions have no fixed wave number their structure in the nonlinear regime may gradually evolve from resembling a solution with  $n$  maxima to one with  $n + 1$  maxima, say; no bifurcation is involved and no periodic solutions are present. It follows that the snaking branches cannot terminate on a branch of periodic states and another termination mechanism must be present. The present paper describes in some detail what happens in this case. The results are quite general and provide an immediate explanation of the behavior identified in Ref. [15]. In addition, the results should apply to any physical system with realistic lateral boundary conditions and as such should be observable not only in numerical studies of snaking systems with realistic lateral boundary conditions but also in experiments.

This paper is organized as follows. In the next section we summarize briefly the snaking behavior for the Swift-Hohenberg equation on periodic domains. In Sec. III we introduce a homotopy parameter that allows us to continuously change the boundary conditions away from Neumann boundary conditions and explore the accompanying changes in the snaking structure. In Sec. IV we give partial results on other types of boundary conditions. In Sec. V we relate our findings to earlier work on convection in binary fluid mixtures with thermally conducting no-slip lateral boundary condi-

tions where snaking without bistability was first identified [15].

## II. SWIFT-HOHENBERG EQUATION

The Swift-Hohenberg equation describes the formation of spatially periodic patterns with a finite wave number  $k_0$  at onset. In one spatial dimension the equation takes the form

$$u_t = ru - (\partial_x^2 + k_0^2)^2 u + f(u). \tag{1}$$

This equation is variational and hence on finite domains all solutions approach steady states. In the following we shall be interested in characterizing such states. The key to the properties of these states is provided by the invariance of Eq. (1) under  $x \rightarrow -x, u \rightarrow u$ , hereafter referred to as *reversibility*. On the real line this property is responsible for the presence of a

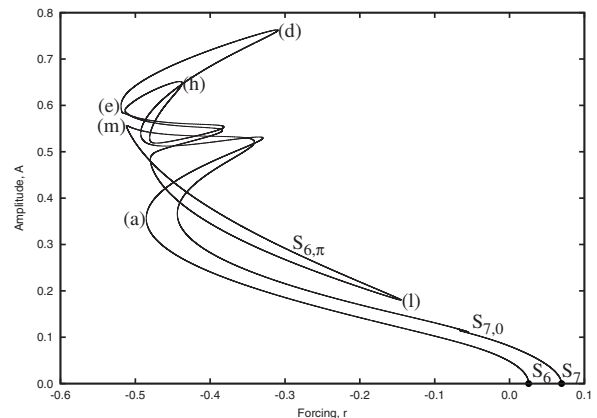


FIG. 9. The  $S_{6,\pi}$  branch for  $\beta=0.5$  on a domain of length  $2L=40$ . The branch connects to  $S_7$  via a complicated sequence of saddle-node bifurcations.

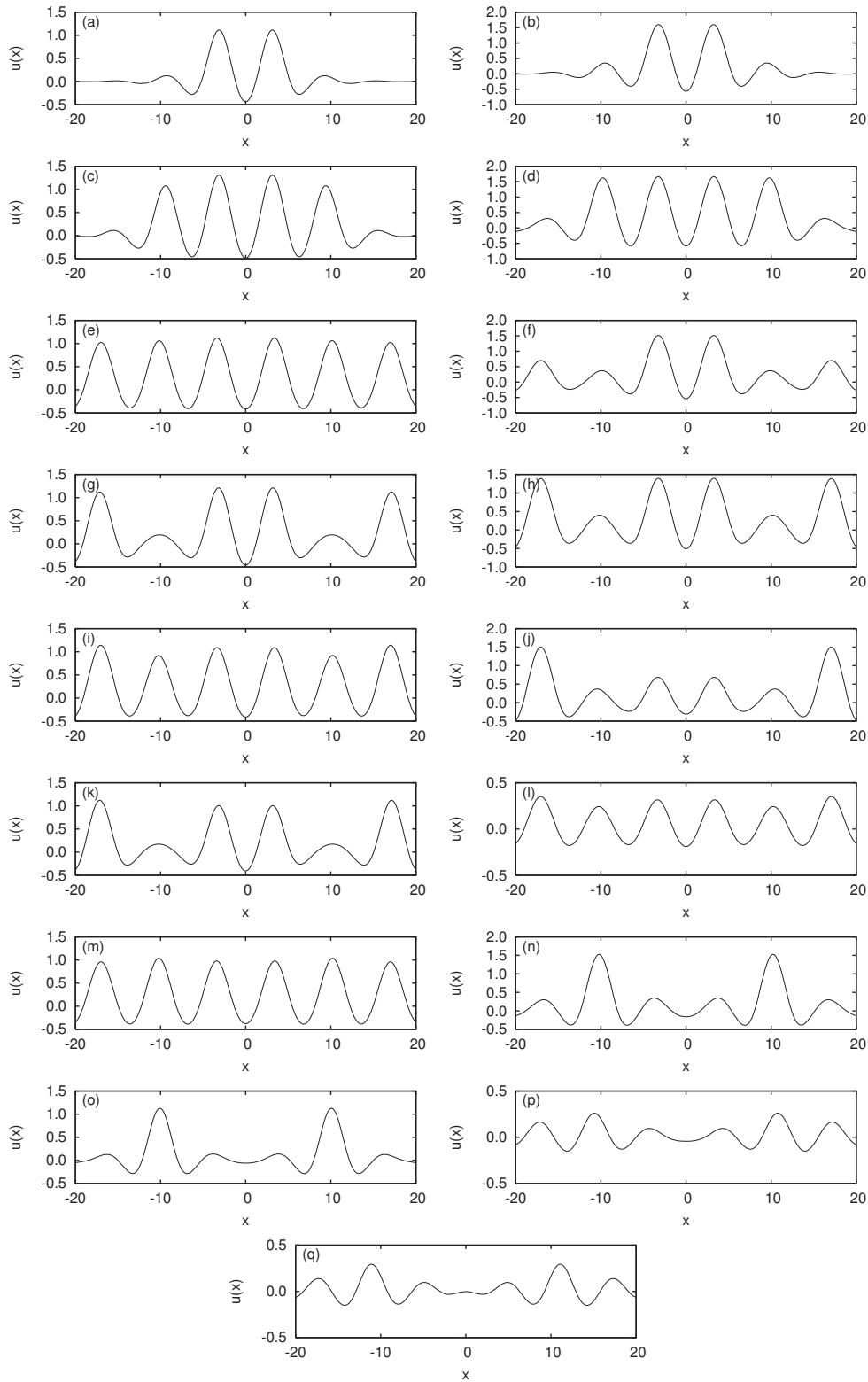


FIG. 10. Solution profiles  $u(x)$  at successive saddle nodes along the  $S_{6,\pi}$  branch in Fig. 9 from small to large amplitude and then back toward small amplitude along the  $S_7$  branch. Parameters:  $\beta=0.5$  and  $2L=40$ .

reversible Hopf bifurcation with 1:1 resonance in the linear stability problem for the trivial solution  $u=0$  in space. Specifically, at  $r=0$  the (four) spatial eigenvalues are given by  $\lambda = \pm ik_0$ , each with double multiplicity. Moreover, for  $r < 0$  these eigenvalues move off the imaginary axis and form a

complex quartet  $\{\lambda = \pm [ik_0 \pm (\sqrt{-r}/2k_0) + \mathcal{O}(r)]\}$ , while for  $r > 0$  they also split but remain on the imaginary axis  $\{\lambda = \pm [ik_0 \pm i(\sqrt{r}/2k_0) + \mathcal{O}(r)]\}$ . The presence of this bifurcation can in turn be used to show that spatially periodic and spatially localized states bifurcate *simultaneously* from  $u=0$

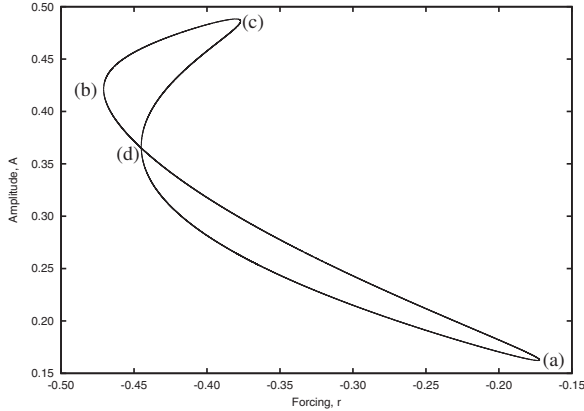


FIG. 11. The isola of two-pulse  $\phi=\pi$  states computed for  $\beta=0.5$  and  $2L=40$ . A similar isola of  $\phi=0$  states is omitted.

as the bifurcation parameter  $r$  is increased through  $r=0$  only in the so-called *subcritical* regime [1,10]. The latter undergo the homoclinic snaking that is of interest in the present paper.

In this paper we consider the case  $f(u) \equiv b_2 u^2 - u^3$ , which is the simplest nonlinearity that produces the bistability crucial for homoclinic snaking. In the following we scale Eq. (1) such that  $k_0=1$  so that the equation is fully parametrized by  $r$  and  $b_2$  and explore the case  $b_2=2$ , focusing on steady state solutions in finite domains. Throughout we impose boundary conditions at  $x = \pm L$  and do so in such a way that the invariance of system (1) under reflections  $x \rightarrow -x$  is preserved. In this case general theory [20] guarantees the presence of nonlinear even-parity solutions. Figure 2 shows several branches of such even-parity states with Neumann boundary conditions at  $x = \pm 20$  or, equivalently, in a periodic domain with period  $4L=80$ . The figure shows the amplitude  $A = \|u\|_{L^2} \equiv (1/2L)^{-1} \int_{-L}^L u^2(x) dx$  for two branches, labeled as  $P_6$  (six peaks within the domain) and  $P_5$  (five peaks), both of which bifurcate from the trivial state  $u=0$ ; a branch  $P_7$  bifurcates from  $u=0$  between these two primary branches but is not shown. Both  $P_6$  and  $P_5$  bifurcate subcritically and turn around to larger values of  $r$  with increasing amplitude. Sample large amplitude solutions on these branches are shown in Fig. 3. The figure also shows a pair of snaking branches both of which bifurcate from  $P_6$  at small amplitude

and terminate back on  $P_6$  just below the saddle node. These correspond to localized structures with maxima ( $\phi=0$ ) and minima ( $\phi=\pi$ ) at  $x=0$ , respectively. An isola of two-pulse homoclinic orbits is also shown, with sample profiles shown in Fig. 4. These results accord with the results in [12,21,22].

### III. ROBIN BOUNDARY CONDITIONS

In this section we explore the effect of changing the boundary conditions at  $x = \pm L$  to

$$u_x = \pm \beta u, \quad u_{xxx} = 0, \quad (2)$$

where the parameter  $\beta$  plays the role of a Biot number: the case  $\beta=0$  corresponds to the NBC case, while  $\beta \neq 0$  corresponds to RBC.

#### A. Numerical method

We solve for steady solutions of Eq. (1), subject to the boundary conditions (2), using the Newton-Raphson-Kantorovich (NRK) algorithm [23]. This algorithm is highly efficient for finding the solution to linear and nonlinear problems. Also, it is straightforward to incorporate the nonstandard boundary conditions as required for this investigation. We initialize the algorithm with an approximate solution and then apply NRK to converge to an exact solution of the linear or nonlinear problem. A parameter in the system is then slightly altered and NRK used once more to converge to an exact solution. Repetition of this procedure allows the solution branches to be traced out. Other numerical algorithms, for example, AUTO [24], could also be used. AUTO allows nonstandard boundary conditions to be specified in the BCND subroutine so that boundary value problems of this type can be solved.

#### B. Linear theory

When  $\beta=0$  the neutral stability curves for the trivial state  $u=0$  are given by

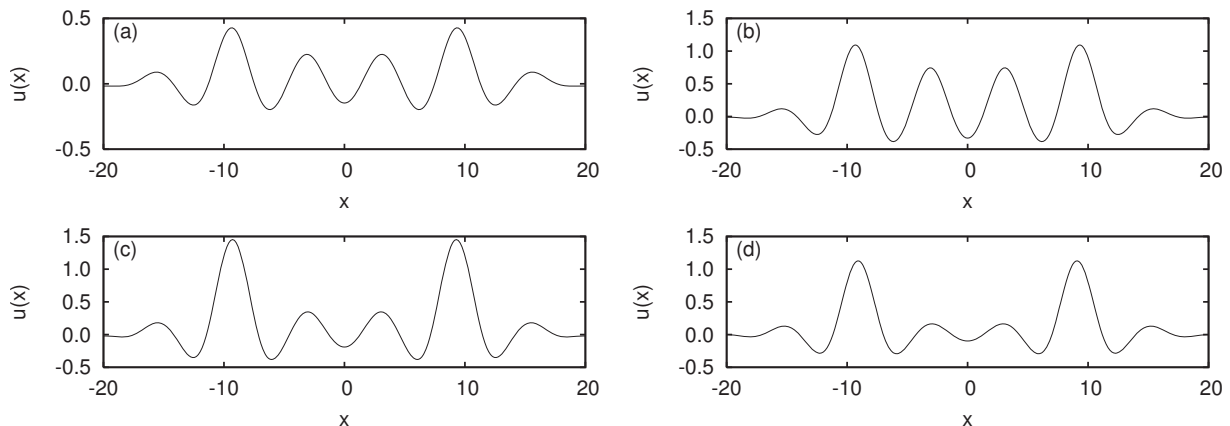


FIG. 12. Solution profiles  $u(x)$  at successive saddle nodes along the two-pulse isola in Fig. 11 when  $\beta=0.5$  and  $2L=40$ .

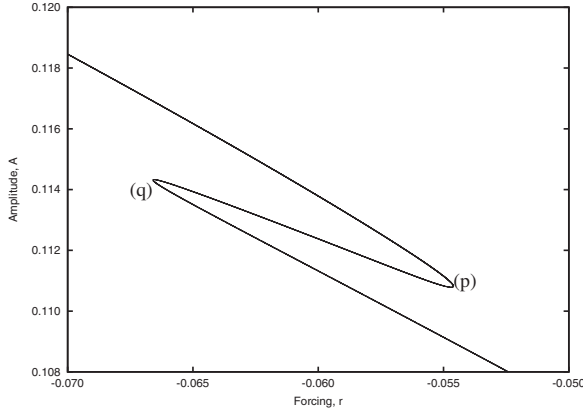


FIG. 13. A blow-up of the region on the  $S_{7,0}$  branch (Fig. 9) showing a pair of saddle-node bifurcations created from an imperfect bifurcation. Solution profiles (p) and (q) are shown in Fig. 10.

$$r_c^{\text{even}} = \left[ 1 - \left( \frac{n\pi}{L} \right)^2 \right]^2, \quad r_c^{\text{odd}} = \left[ 1 - \left( \frac{(2n+1)\pi}{2L} \right)^2 \right]^2. \quad (3)$$

There are two sets of curves corresponding to even  $[\cos \pi x/2L]$  and odd  $[\sin(2n+1)\pi x/2L]$  eigenfunctions with well-defined wave numbers specified by integers  $n=0, \dots$  as shown in Fig. 5(a). As soon as  $\beta \neq 0$  this picture changes dramatically, as described in [19] and references therein: the crossings between even neutral curves breakup, as do the crossings between odd neutral curves. Only crossings between opposite parity neutral curves are structurally stable. The resulting neutral curves are shown in Fig. 5(b) for a relatively large value of  $\beta$ ,  $\beta=0.5$ . The figure shows five distinct families of neutral curves, each of which consists of a pair of braided curves, one of which corresponds to even-parity eigenfunctions (red solid), while the other corresponds to odd-parity eigenfunctions (blue dashed). As a result of the reconnection between neutral curves corresponding to different values of  $n$  the neutral curves with RBC are no longer characterized by a unique mode number, and the mode num-

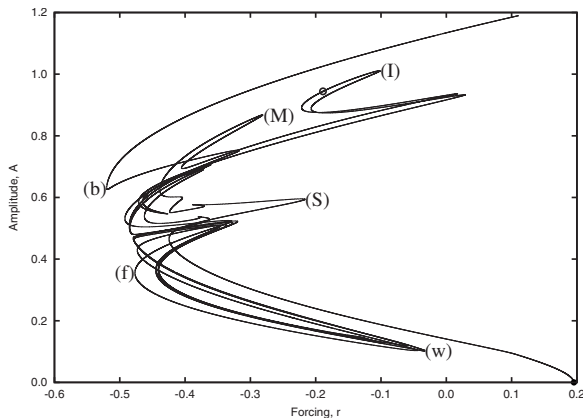


FIG. 14. Bifurcation diagram for  $\beta=0.5$  and  $L=20$  showing the large amplitude  $\phi=\pi$  branch. This branch becomes disconnected from the smaller amplitude  $\phi=\pi$  branch  $S_{6,\pi}$  shown in Fig. 9 near (b) but connects to a subsequent primary bifurcation at  $S_5$ .

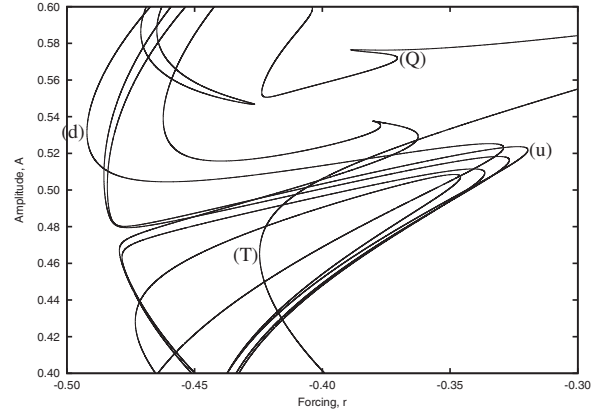


FIG. 15. Detail of Fig. 14.

ber varies continuously along each neutral curve.

The bifurcations to even modes produce branches of even-parity nonlinear solutions. We construct these solutions by imposing the boundary conditions

$$u_x = 0, \quad u_{xxx} = 0, \quad (4)$$

at  $x=0$ , and solving for steady solutions on  $0 \leq x \leq L$  with the boundary conditions (2,4), followed by a reflection in  $x=0$ :  $u(-x)=u(x)$ . This procedure generates a differentiable solution on the full domain  $-L \leq x \leq L$ . However, because of the quadratic term in the Swift-Hohenberg equation odd-parity states do not persist into the nonlinear region; these bifurcations produce primary branches of *nonsymmetric* states, and these have to be computed on the full domain  $-L \leq x \leq L$ . When  $\beta \neq 0$  none of these solutions is characterized by a well-defined mode number  $n$ , and as a result the dominant mode number will in general be a function of amplitude or equivalently of the value of the parameter  $r$ .

### C. Even-parity states

The bifurcation diagram for the primary even-parity states is shown in Fig. 6 for  $\beta=0.5$  and  $L=20$ . We refer to this branch as  $S_{6,0}$  since it starts out looking like a  $P_6$  state with maxima at  $x=0$ ; like  $P_6$  it bifurcates subcritically and starts to snake but then turns around unexpectedly toward *larger* values of  $r$ .

To understand this dramatic change in the bifurcation diagram (compare Figs. 2 and 6), we need to go back to the primary bifurcation. As already mentioned, with PBC on a domain with period  $4L$  the primary bifurcation is a pitchfork of revolution. The imposition of NBC at  $x = \pm L$  selects from these solutions a pair of solutions. These are related by a translation present within the PBC formulation; this translation manifests itself as a “hidden” symmetry within the NBC case [16] and explains why the solutions in the NBC case remain sinusoidal with well-defined wave numbers instead of just being odd or even under reflection in  $x=0$ . These observations also explain why the primary bifurcation is a pitchfork even when the solution is even under reflection in  $x=0$ . When  $\beta$  becomes nonzero this hidden symmetry is broken and the bifurcation becomes generic: bifurcations to odd solutions (in  $x=0$ ) remain pitchforks, while the even ones

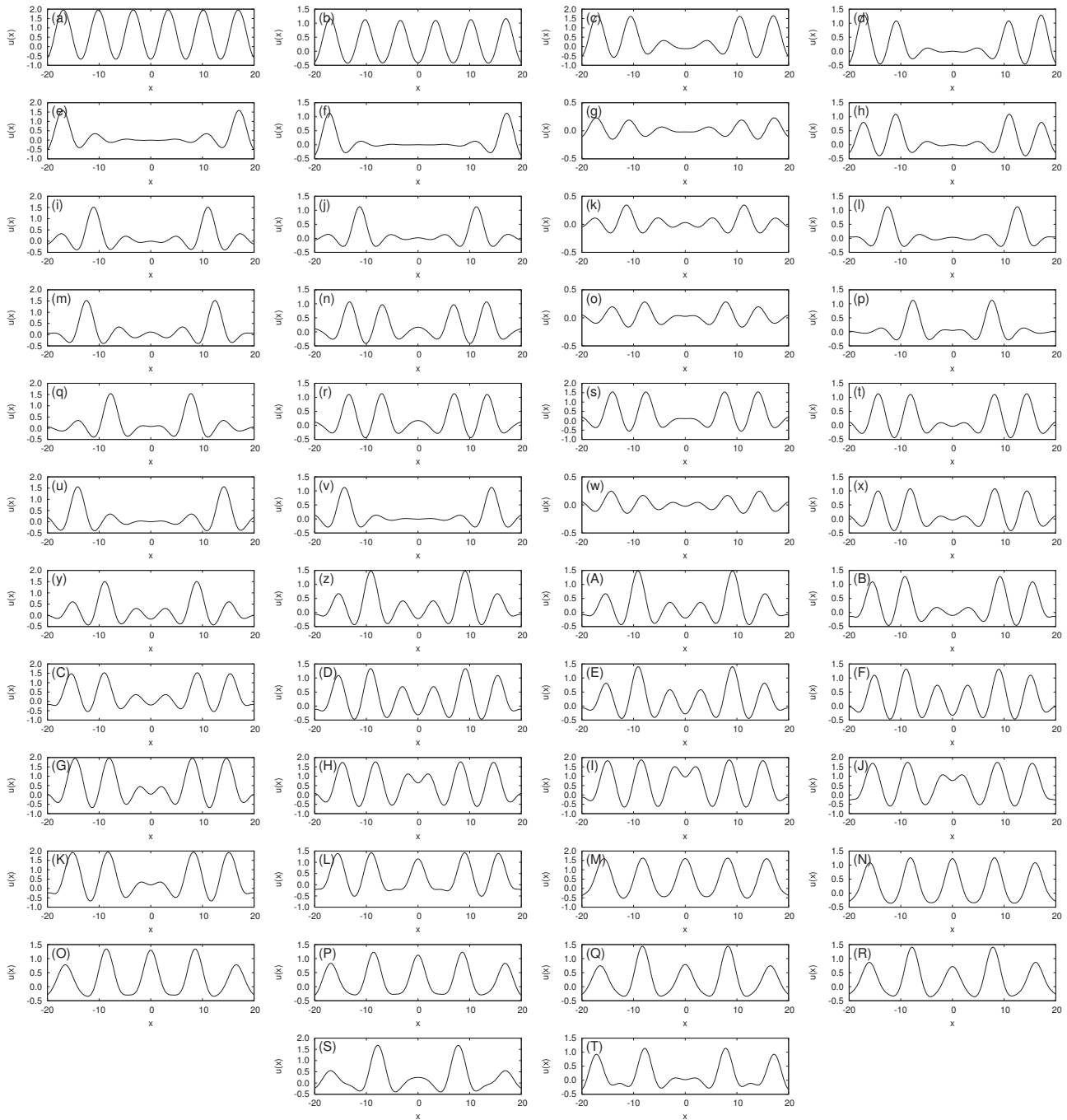


FIG. 16. Solution profiles  $u(x)$  at successive saddle nodes in Fig. 14 (and Fig. 15), starting from the large amplitude  $P_6$  state (a) and finishing at the last saddle node (T) before the primary bifurcation at  $S_5$ .

(such as  $S_6$  and  $S_5$ ) become transcritical, hereafter indicated by solid dots. Figure 7(a) confirms this expectation, while Fig. 7(b) shows that the loss of the hidden symmetry also affects the pitchfork bifurcations at finite amplitude that are responsible for the appearance of the pair of branches of localized states in the NBC case: the structure shown evolves continuously from the pitchfork bifurcations on  $P_{6,0}$  and  $P_{6,\pi}$  when  $\beta=0$  as  $\beta$  increases from zero.

As the amplitude of both  $S_{6,0}$  and  $S_{6,\pi}$  increases the solutions begin to resemble more and more the localized states familiar with Neumann boundary conditions, and both solu-

tion branches begin to snake. Figure 8 shows the states at successive saddle nodes along the  $\phi=0$  branch. Except for the behavior near  $x = \pm L$  we observe classic homoclinic snaking, with structures added symmetrically on either side with increasing amplitude, gradually filling the domain. However, instead of turning over toward smaller values of  $r$  and terminating on a branch of periodic states as in Fig. 2 the branch turns instead toward larger  $r$  and takes the place of the large amplitude periodic states. The final panel in Fig. 8 shows the resulting large amplitude  $\phi=0$  state. This state resembles the defect states identified in [12] that bifurcate

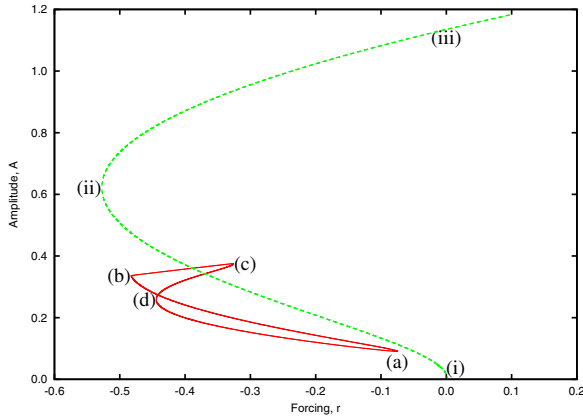


FIG. 17. (Color online) Bifurcation diagram for the case  $\beta=0$ ,  $L=20$ . The pattern mode  $A_6$  (green dashed) is shown together with the lowest of a stack of figure-eight isolas (red solid). Sample solution profiles are shown in Figs. 18 and 19.

from the periodic states in Eckhaus or sideband bifurcations: here the defect takes the form of a hole in an otherwise almost periodic pattern located at  $x = \pm L$ .

The  $\phi = \pi$  branch  $S_{6,\pi}$  is shown in Fig. 9. As already mentioned this branch bifurcates from  $S_6$  initially supercritically but turns around at small amplitude and then undergoes many back and forth gyrations before returning to small amplitude and terminating at the primary bifurcation point  $S_7$ . Thus once  $\beta \neq 0$  the  $S_6$  solutions with minima at  $x=0$  transform continuously into solutions with seven peaks and maxima at  $x=0$  resembling  $P_7$ . The details of this transformation are shown in Fig. 10. We see that the  $S_{6,\pi}$  branch enters the snaking region at saddle node (a) [Fig. 10(a)] with two peaks, acquires two additional peaks at saddle node (c) [Fig. 10(c)], and then fills the domain at saddle node (e) [Fig. 10(e)], where the solution resembles the finite amplitude periodic  $P_6$  state. In between saddle nodes (e) and (f) the branch develops holes near  $x = \pm L$  before filling them in by saddle node (i) where it resembles  $P_6$  again [Fig. 10(i)]. Between saddle nodes (i) and (j) the solution again develops a hole, but this time centered on  $x=0$ , before undergoing a large excursion toward small amplitudes that takes it back to  $P_6$  at saddle node (m) [Fig. 10(m)]. Beyond this point the solution develops deep holes near both  $x=0$  and  $x = \pm L$ , and with decreasing amplitude the central minimum becomes a

maximum and the solution evolves into a  $S_{7,0}$  state with seven peaks and a maximum at  $x=0$  by the time it reconnects with the  $u=0$  state at  $S_7$ .

To complete the picture we show in Fig. 11 the two-pulse isola computed for  $\beta=0.5$ . The corresponding profiles are shown in Fig. 12.

To understand how it is possible for a small amplitude localized  $\phi=0$  state to turn via snaking into a large amplitude defect state without undergoing any bifurcations at all, we need to examine the fate of the secondary bifurcations creating the  $\phi=0, \pi$  snaking branches when  $\beta=0$ . Both bifurcations are pitchforks. This is a consequence of weak spatial resonance [12] and not reflection symmetry and is the case for the bifurcations from both  $\phi=0$  and  $\phi=\pi$  periodic states. Thus while Fig. 2 shows only one pitchfork bifurcation with two emerging branches, there are in fact two pitchforks and four emerging branches and likewise at the termination points. When  $\beta \neq 0$  we expect these pitchforks to become imperfect bifurcations; for given  $\beta \neq 0$  this effect should be larger for the small amplitude pitchforks and smaller for the larger amplitude pitchforks. Moreover, the universal unfolding of the pitchfork bifurcation [25] reveals the presence of an additional disconnected branch as well. The predicted splitting of the termination pitchfork on the  $\phi=\pi$  branch is clearly seen in Fig. 9 and manifests itself in the two distinct hole states created between saddle nodes (e) and (f) and between (m) and (n) (Fig. 10). On the other hand for  $\beta=0.5$  the break up of the small amplitude pitchfork is much more substantial, although the saddle node (l) [Figs. 7(b) and 9] and the small oscillation in the  $S_{7,0}$  branch (enlarged in Fig. 13) are clearly related to the unfolding of a pitchfork (which for these large values of  $\beta$  involves  $S_{7,0}$  instead of  $S_{6,\pi}$ ). The disconnected  $\phi=0$  branch in Fig. 7(b) lies on an isola (not shown) that is quite similar to that in Fig. 11 and the corresponding profiles are similar to those in Fig. 12 except that they resemble the  $\phi=0$  seven peak state instead of the  $\phi=\pi$  six peak state (not shown).

Figure 9 shows that the  $\phi=\pi$  branch originating at  $S_6$  does not extend to large amplitude and instead connects to  $S_7$ . The reconnection between the  $S_{6,\pi}$  and  $S_{7,0}$  branches indicates that there is a disconnected  $\phi=\pi$  branch that is missing from Fig. 9, a conclusion confirmed in Fig. 14. Figures 15 and 16 provide details of the transition from large to small amplitude behavior along this branch. We see that this branch likewise undergoes numerous saddle-node bifurca-

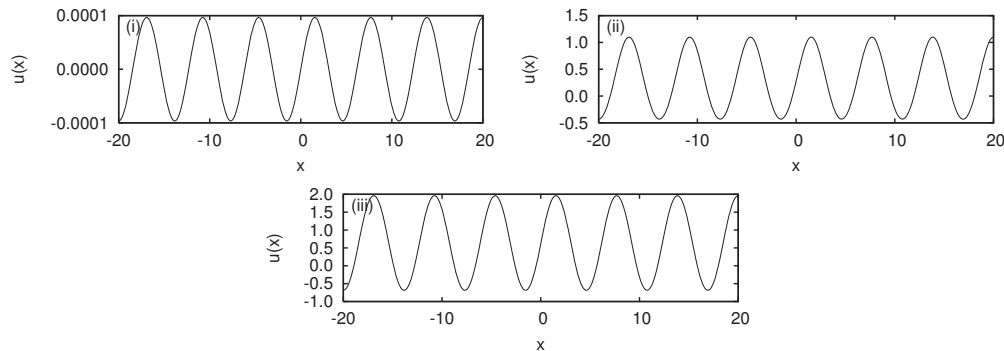
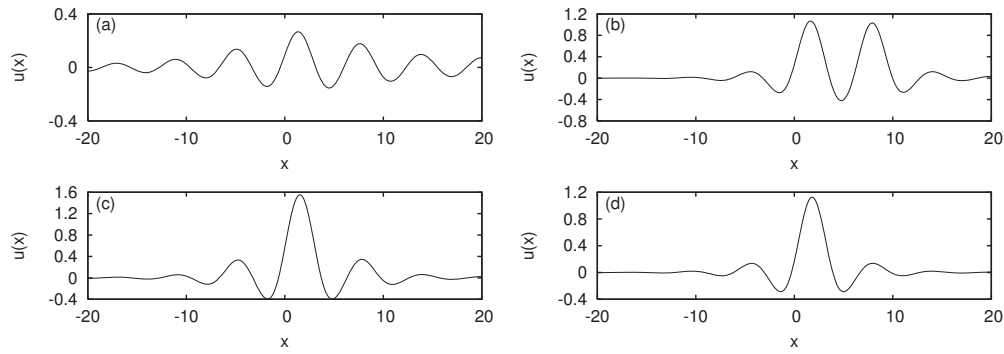


FIG. 18. Solution profiles  $u(x)$  on the branch  $A_6$  in Fig. 17 at (i) small amplitude, (ii) the saddle node and (iii) large amplitude. The mean of the solution increases monotonically with amplitude.

FIG. 19. Solution profiles  $u(x)$  at each of the saddle nodes on the figure-eight isola shown in Fig. 17.

tions within the original snaking region before terminating on  $u=0$  at a subsequent primary bifurcation. During this transition the solution changes continuously from essentially  $P_6$  at large amplitude [Fig. 16(a)] to essentially  $P_5$  [Fig. 16(M)]; in between we observe the development of very clear holelike states [Figs. 16(f) and 16(v)] and the gradual filling in of the hole as one proceeds down the branch [e.g., Fig. 16(x)]. Such states are expected as a result of the splitting of the branches of holelike states near the saddle node on  $P_6$  and their reconnection with the original  $P_6$  branch when  $\beta \neq 0$ .

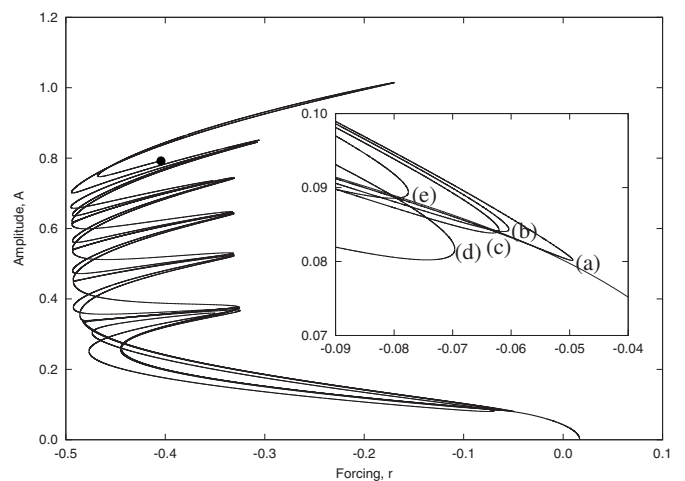
#### D. Nonsymmetric states

The linear stability problem shows that the trivial state  $u=0$  loses stability to both even and odd modes. Thus far we have discussed the nonlinear states associated with even eigenfunctions. In this section we turn to the states associated with odd eigenfunctions. Since Eq. (1) does not admit odd-parity solutions such eigenfunctions must produce *nonsymmetric* states in the nonlinear regime.

Figure 17 shows the first branch of nonsymmetric states when  $\beta=0$  and  $L=20$ . This branch, hereafter  $A_6$ , consists of spatially extended states that are almost antisymmetric with respect to a nonzero mean (Fig. 18) and precedes the first primary bifurcation to an even-parity state [Fig. 5(a)]. Spatially localized states (Fig. 19) are also present but are confined to a stack of figure-eight isolas of which only the lowest is shown in Fig. 17. Since the figure is computed with NBC ( $\beta=0$ ) the associated localized profiles can be reflected in the boundary at  $x=-L$  or  $x=L$  without generating a non-differentiable state. Such states therefore solve the PBC problem and evidently correspond to two-pulse states on a periodic domain of period  $4L$ . On the real line the resulting replicated state consists of a train of pulses with alternating separations  $d_1$  and  $d_2$ , with  $d_1 \neq d_2$ . For the Swift-Hohenberg equation with PBC states of this type are well known, and it is known that such states lie on figure-eight isolas whenever  $d_1 \neq d_2$  [22].

When  $\beta=0.5$  and  $L=20$  the bifurcation to the nonsymmetric states  $A_6$  in Fig. 20 also precedes the first bifurcation to even-parity states [Fig. 5(b)]. The figure shows that  $A_6$  bifurcates subcritically, enters the snaking region, and starts to snake toward larger amplitude but turns around immediately to form a figure-eight structure characteristic of two-

pulse states (Fig. 17). It then continues upwards along the snaking structure taking in all the rung states (after all, this is a branch of nonsymmetric states) before turning around at the top and descending again. The net effect is that the same branch follows *all* parts of the snake-and-ladders structure of the pinning region. Once it reaches the bottom it describes a new and distinct figure-eight structure and then heads once again up the snaking structure. Apparently this process repeats a number of times, and the distinct braids created in this manner correspond to slightly different locations of the dominant peaks in the solution profile. The inset shows, as expected, that there are no secondary bifurcations responsible for the creation of localized states although there are in fact five saddle nodes in this region, two of which arise from the unfolding of the pitchfork bifurcations that are present in this region with NBC. Three of the curves shown in the inset come from the reconnection of the primary branch with distinct two-pulse isolas in the NBC case such as the one shown in Fig. 17. Figure 21 shows the solution profiles at the saddle nodes in this region; if reflected in  $x=L$  the first three of these generate distinct two-pulse states on an approximately periodic domain of length  $4L$ , i.e., two-pulse states with dif-

FIG. 20. Bifurcation diagram for  $\beta=0.5$  and  $L=20$  showing the branch  $A_6$  of nonsymmetric states. The branch is continuous and follows all parts of the snake-and-ladders structure of the pinning region, and does so several times. The filled circle at large amplitude denotes the point at which continuation of the branch was stopped.

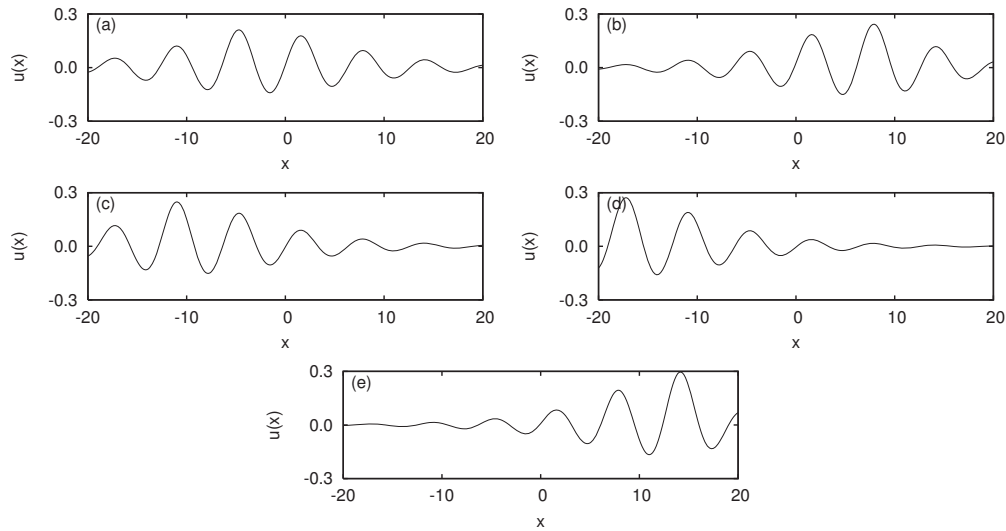


FIG. 21. Solution profiles  $u(x)$  at the five saddle nodes visible (right to left) in the inset in Fig. 20. The first three are related to distinct two-pulse states present with NBC.

ferent separations between the two dominant peaks.

In Fig. 22 we show the branch  $A_5$  that bifurcates from  $u=0$  at a larger value of  $r$ . We see that this branch also bifurcates subcritically, enters the snaking region, and follows some of the rung states to large amplitude. However, this time the branch terminates at finite amplitude on an even-parity branch, the branch  $S_{5,0}$ . Figure 23 shows the evolution of the solution profiles, starting at small amplitude (top left panel) where the solution is almost exactly antisymmetric and ending on the even-parity branch  $S_{5,0}$ . The figure shows that as the amplitude increases the degree of asymmetry gradually decreases, allowing the initially odd-parity state to terminate in an even-parity state. The process whereby this happens is related to the orientation-turning states that are generated in other problems of this type through the breaking of a reflection symmetry. In [26] such states are produced by perturbing the symmetry  $O(2)$  of a circular domain to the symmetry  $Z_2 \times Z_2$  of an elliptical domain. In the present problem the PBC problem also has  $O(2)$  symmetry, and this symmetry is broken by the use of RBC leaving a  $Z_2$  symmetric problem.

IV. OTHER BOUNDARY CONDITIONS

The boundary conditions (2) at  $x=L$  and (4) at  $x=0$  also reduce to Neumann boundary conditions when  $\beta=0$ . Even parity  $\beta \neq 0$  can therefore be related to the solutions of the corresponding PBC problem with spatial period  $4L$  by examining in detail the effect of breaking the hidden symmetry that is present when  $\beta=0$  and that is responsible for the nongeneric behavior of even states in this type of problem. In this section we examine what happens with other boundary conditions, and in particular with boundary conditions that are “far” from the NBC case. To this end we choose the boundary conditions

$$u_x = u_{xxx} = 0 \quad \text{at} \quad x = 0,$$

$$u_x - \beta u = u_{xx} = 0 \quad \text{at} \quad x = L, \tag{5}$$

and focus on even solutions only. Figure 24 shows the bifurcation diagram when (a)  $\beta=0, L=35$ , (b)  $\beta=1, L=35$ , and (c)  $\beta=1, L=40$ .

This type of structure persists for larger  $\beta$  values as well. Figure 25(a) shows the bifurcation diagram for  $\beta=10$ . Only the  $\phi=0$  branch is shown; the  $\phi=\pi$  branch is shown in Fig. 25(b). Observe that, as in earlier cases, the  $\phi=0$  branch snakes toward large amplitude before snaking back down, and almost reaching zero amplitude, before returning to large amplitudes and exiting the snaking region toward large  $r$ . Once again, many of the features of this bifurcation diagram can be understood as the result of the unfolding of the pitchfork bifurcations at the beginning and end of the snaking branches, as well as those responsible for the rungs in the snakes-and-ladders structure of the pinning region. Note,

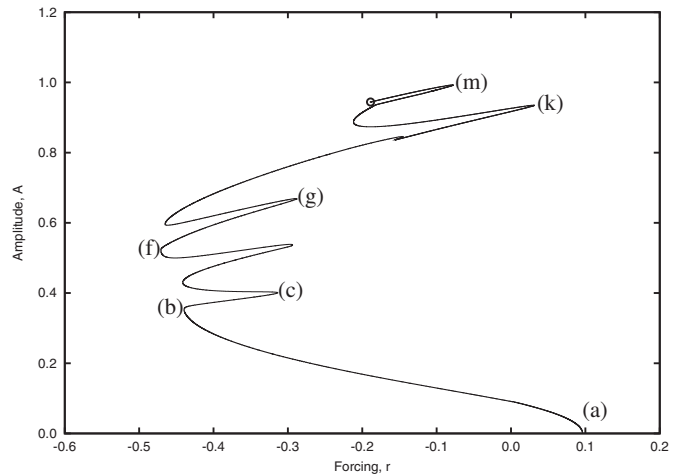


FIG. 22. Bifurcation diagram for  $\beta=0.5$  and  $L=20$  showing the branch  $A_5$  of nonsymmetric states until the branch terminates on the  $S_{5,0}$  branch at (O). This point is also marked on Fig. 14 for comparison. Solution profiles at each saddle node are shown in Fig. 23.

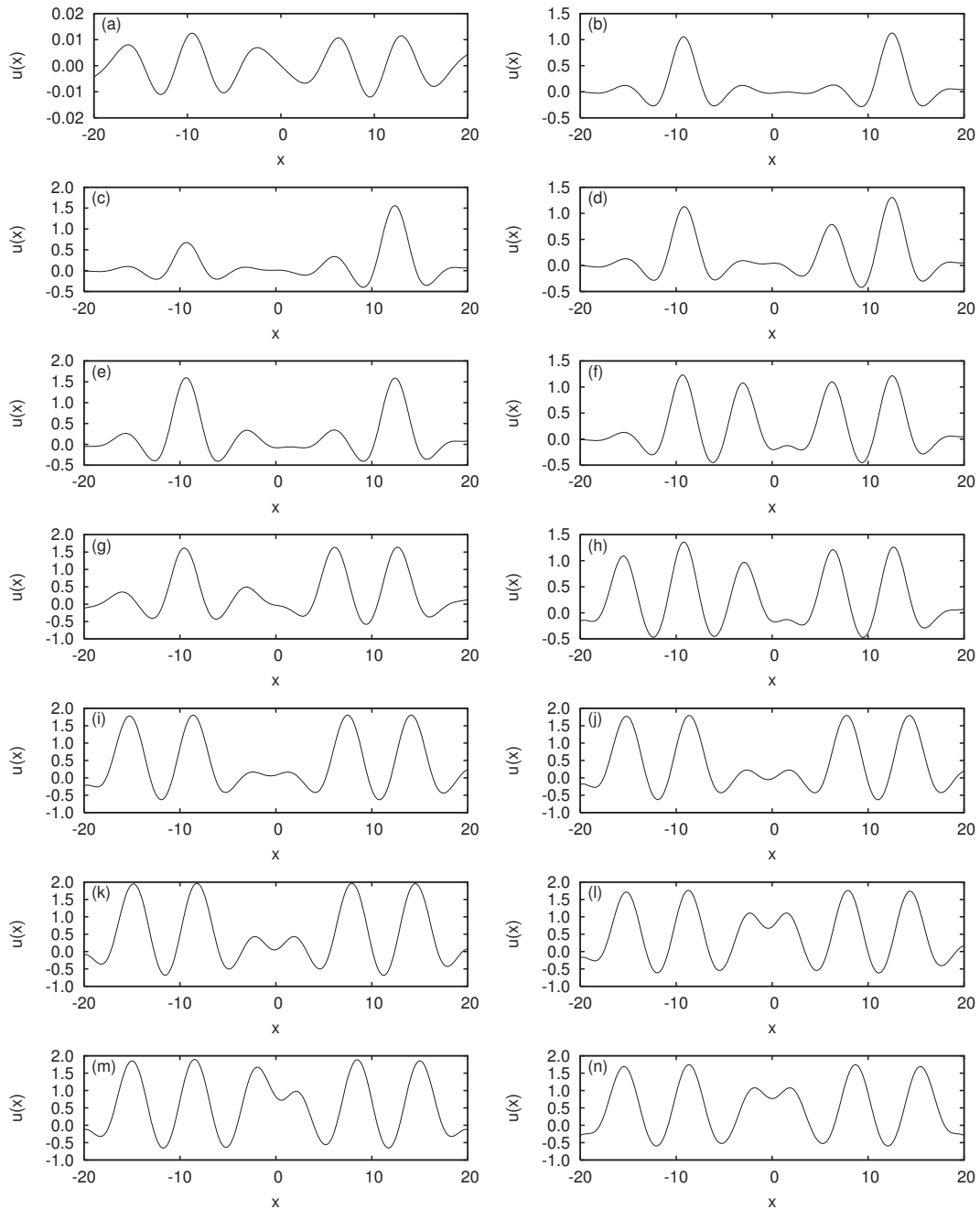


FIG. 23. Solution profiles  $u(x)$  at successive saddle nodes in Fig. 22 starting near the first bifurcation and ending at the termination of  $A_5$  on the even-parity branch  $S_{5,0}$ .

however, that the solutions corresponding to the rungs are now symmetric with respect to  $x=0$ . In contrast, the  $\phi=\pi$  branch forms an isola: the branch is disconnected from both the  $u=0$  state and no longer extends to large amplitude. Note that the pair of saddle nodes where the branch might be expected to connect to a periodic state [top left in Fig. 25(b)] is of the type expected from the breakup of a pitchfork bifurcation [25]. Sample  $\phi=0$  solution profiles are shown in Fig. 26; the two-pulse profiles correspond to either end of the first rung state (in the direction of increasing amplitude) and form when the snaking branch reconnects with a two-pulse isola. There is another  $\phi=\pi$  branch as well. This branch

bifurcates from the trivial state at the same location as the  $\phi=0$  branch and does extend to large amplitude at large  $r$  (not shown).

It appears that much of the structure of the bifurcation diagrams visible at large amplitude is due to the choice of the domain length  $2L$  and its commensurability with the basic wavelength  $\lambda=2\pi$  selected by the linear operator. For example, when  $L=40$  this structure is absent [Fig. 24(c)].

### V. DISCUSSION AND CONCLUSIONS

In this paper we have examined the phenomenon of homoclinic snaking in the presence of realistic boundary con-

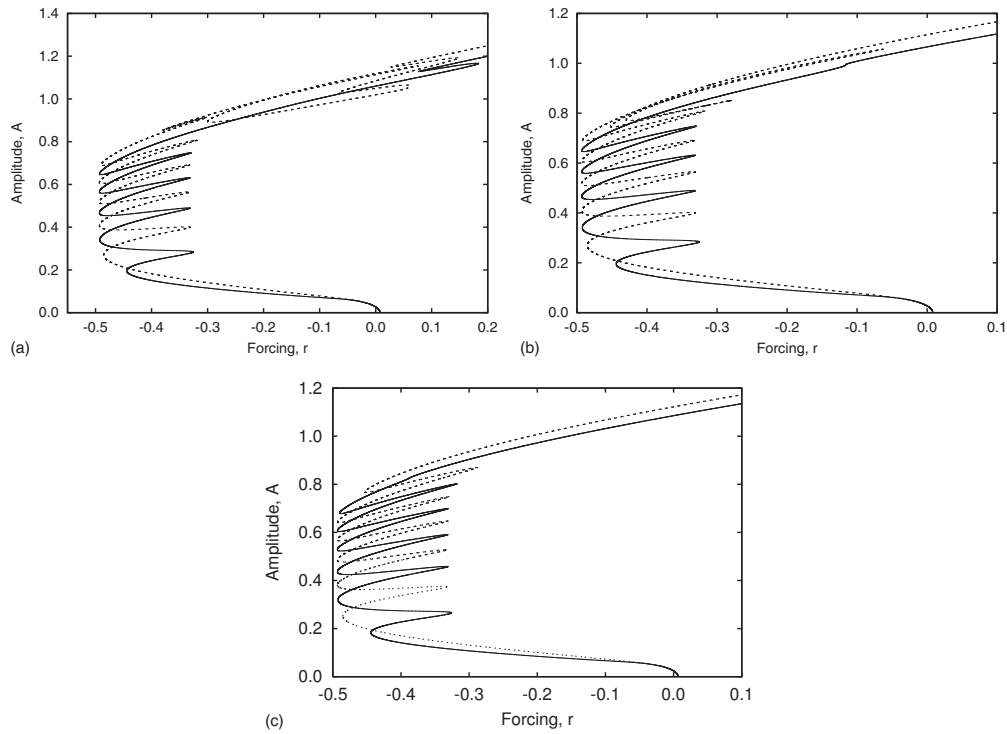


FIG. 24. Bifurcation diagrams with boundary conditions (5) for (a)  $\beta=0, L=35$ , (b)  $\beta=1, L=35$ , and (c)  $\beta=1, L=40$ . Solid (dashed) lines indicate  $\phi=0, \pi$  states, respectively. Only even-parity states are shown.

ditions. Existing studies of homoclinic snaking employ periodic boundary conditions with a large spatial period to model problems on the real line. Provided the localized structures that are of interest do not fill the domain (i.e., provided they do not approach to within half a wavelength of the imposed boundaries on either side) the presence of boundaries has a small effect on the behavior of the solutions. In a recent paper Bergeon *et al.* [12] have examined the consequences of breaching this requirement. This occurs close to the primary bifurcation to localized states since the corresponding eigenfunction takes the form of a periodic wave train modulated on a long scale and again at large amplitude when the domain is filled with the structured state. In either case snaking must terminate and Bergeon *et al.* explore in detail the process by which this happens (see also [13]). Within the Swift-Hohenberg equation the snaking branches always terminate on one of the branches of spatially periodic states and do so near a saddle-node bifurcation.

In this paper we have shown that this scenario changes fundamentally when periodic or Neumann boundary conditions are changed to Robin boundary conditions. These boundary conditions eliminate the large amplitude spatially periodic states, whose role is taken by states that necessarily include defectlike structures near either boundary. In fact there are two branches of such states distinguished by their spatial phase  $\phi$  since the boundary conditions split the branch of periodic states satisfying Neumann boundary conditions. In addition, the  $\phi=0, \pi$  snaking branches now bifurcate directly from  $u=0$  and no longer at small amplitude no longer terminate at secondary bifurcations. Instead, one of these, typically the first one, develops smoothly and continuously into a large amplitude branch with the corresponding spatial phase, while the second snaking branch instead turns over toward smaller amplitude and reconnects with the trivial state  $u=0$  in a subsequent primary bifurcation also split by the boundary conditions. There is in addition a sec-

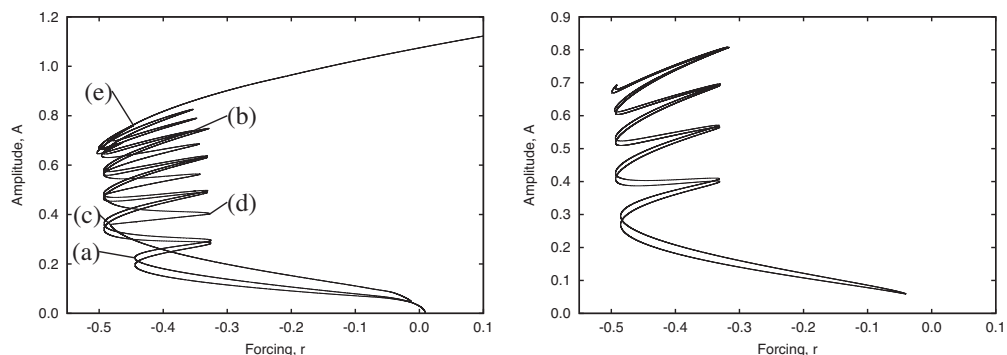


FIG. 25. Bifurcation diagrams with the boundary conditions (5) for  $\beta=10$  and  $L=35$ . (a)  $\phi=0$  and (b)  $\phi=\pi$  (isola only).

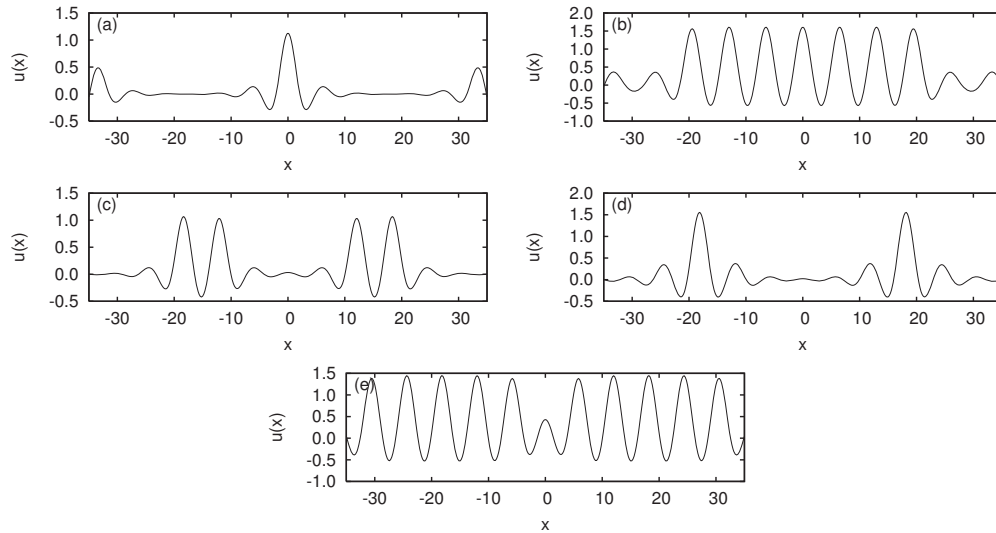


FIG. 26. Solution profiles  $u(x)$  for the boundary conditions (5) with  $\beta=10$  and  $L=35$  at the saddle nodes indicated in Fig. 25(a).

and large amplitude defect branch, which may reconnect with subsequent large amplitude branches, remaining disconnected from the trivial state. The entire scenario may be viewed as the result of a perturbation of the secondary pitchfork bifurcations (here a consequence of hidden symmetry associated with Neumann boundary conditions [16]) terminating the snaking branches in the NBC case into imperfect bifurcations when the boundary conditions are perturbed to Robin boundary conditions, together with the associated splitting of branches of periodic states. Of course, with increasing departure from the Neumann boundary conditions the details of the required branch reconnections become more and more difficult to discern, as found in other problems of this type [26,27].

We have demonstrated these results here by explicit computations on the so-called 23 Swift-Hohenberg equation and showed that despite the complexity of the resulting bifurcation diagrams much of the phenomenology of these diagrams can be understood as the result of the splitting of various secondary bifurcations (those originating and terminating the snaking branches as well as the pitchfork bifurcations on the snaking branches responsible for the asymmetric states that form the rungs of the snakes-and-ladders structure of the snaking region). In general such splitting is a consequence of imperfect bifurcations, but if organized by the underlying snaking structure it can result in a stack of isolas (as is the case for two-pulse states, where the imperfection is the result of unequally spaced pulses) or a braided structure generated by a broken hidden symmetry as in Fig. 20. Both possibilities are discussed in [22].

We mention here that snaking branches may turn into large amplitude defect states even in the presence of periodic boundary conditions. This occurs, for example, in natural doubly diffusive convection (Fig. 27 of [12]), where, in certain special parameter ranges, the snaking branch does not terminate on a branch of periodic states but instead exits the snaking region toward *larger* values of the bifurcation parameter, apparently continuing to larger and larger amplitudes. The solutions on this branch take the form of a peri-

odic structure with a defect that is apparently required in order to fit the periodic structure into the imposed spatial period. In this case it is apparently “cheaper” to include a defect in the structure than to change the wavelength of the structure throughout the domain. In this case, however, the defect state coexists with a branch of large amplitude periodic states.

Although we have not computed the stability properties of all the solutions reported here, we have checked that at successive saddle nodes a single eigenvalue passes repeatedly through zero. As a result we expect that positively sloping branches will be stable, as established in detail in [1], and have checked this stability prediction in specific cases by explicit eigenvalue computation and direct integration in time.

It should be emphasized that the effect of RBC is not confined to the elimination of the periodic states and their replacement at large amplitude by the defect states which connect continuously to the snaking branches. We have already noted the splitting of the primary branches and the associated connections between distinct primary bifurcations. But the RBC are also responsible for reconnections within the original snaking region that produce branches which follow the original snaking structure up and down several times before exiting the snaking region. This far-reaching effect of even distant boundaries is unexpected and indicates that substantial care is required to model correctly given physical systems; see also [28].

It is interesting to examine the behavior identified here in connection with more realistic systems which exhibit behavior that appears to be related. As an example we take natural doubly diffusive convection in a two-dimensional vertical rectangular cavity with no-slip boundary conditions on all boundaries and imposed horizontal temperature and concentration gradients [29]. In this paper Ghorayeb and Mojtabi find a number of states resembling those identified here for the Swift-Hohenberg equation with Robin boundary conditions. These include localized cells in the center of the container but also localized cells near one boundary or at both

boundaries. We believe that these states can be understood as the result of broken hidden symmetry that is present with NBC and hence as a “perturbation” of the snaking structure that is known to be present in this system in the presence of PBC in the vertical direction [30]. Similar structures have also been identified in a related system with an imposed horizontal concentration gradient driven by an imposed vertical temperature gradient [31,32].

Binary fluid convection with negative separation ratio promises to provide another potential application. This system develops a competing concentration gradient in response to an applied vertical destabilizing temperature gradient and also exhibits homoclinic snaking [33]. However, in contrast to the Swift-Hohenberg equation this system admits a second reflection symmetry, in addition to spatial reversibility in the horizontal direction. As a result the snaking region consists of four branches, two of which involve even-parity states and

two of which involve odd-parity states. Despite this important difference, when the problem is posed on a finite domain with non-Neumann boundary conditions (thermally conducting no-slip lateral boundaries) computations reveal a continuous transition from a small amplitude state, via snaking, to a large amplitude defect state [15], much as found here for the Swift-Hohenberg equation (Fig. 6). This is the case for both even and odd states, and we surmise that the origin of this behavior is similar.

#### ACKNOWLEDGMENTS

This work was supported by EPSRC-GB under Grant No. EP/D032334/1 (S.M.H.) and the National Science Foundation under Grant No. DMS-0605238 (E.K.). We are grateful to Isabel Mercader for helpful comments.

- 
- [1] J. Burke and E. Knobloch, Phys. Rev. E **73**, 056211 (2006).  
 [2] G. Kozyreff and S. J. Chapman, Phys. Rev. Lett. **97**, 044502 (2006).  
 [3] S. J. Chapman and G. Kozyreff, Physica D **238**, 319 (2009).  
 [4] J. Burke and E. Knobloch, Phys. Lett. A **360**, 681 (2007).  
 [5] D. J. B. Lloyd, B. Sandstede, D. Avitabile, and A. R. Champneys, SIAM J. Appl. Dyn. Syst. **7**, 1049 (2008).  
 [6] D. J. B. Lloyd and B. Sandstede, Nonlinearity **22**, 485 (2009).  
 [7] M. Tlidi, M. Taki, and T. Kolokolnikov, Chaos **17**, No. 3 (2007).  
 [8] E. Knobloch, Nonlinearity **21**, T45 (2008).  
 [9] M. Beck, J. Knobloch, D. J. B. Lloyd, B. Sandstede, and T. Wagenknecht, SIAM J. Math. Anal. **41**, 936 (2009).  
 [10] G. W. Hunt, M. A. Peletier, A. R. Champneys, P. D. Woods, M. A. Wadee, C. J. Budd, and G. J. Lord, Nonlinear Dyn. **21**, 3 (2000).  
 [11] P. Couillet, C. Riera, and C. Tresser, Chaos **14**, 193 (2004).  
 [12] A. Bergeon, J. Burke, E. Knobloch, and I. Mercader, Phys. Rev. E **78**, 046201 (2008).  
 [13] J. H. P. Dawes, SIAM J. Appl. Dyn. Syst. (to be published).  
 [14] Y. Pomeau, Physica D **23**, 3 (1986).  
 [15] I. Mercader, O. Batiste, A. Alonso, and E. Knobloch, Phys. Rev. E **80**, 025201 (2009).  
 [16] J. D. Crawford, M. Golubitsky, M. G. M. Gomes, E. Knobloch, and I. N. Stewart, *Boundary conditions as symmetry constraints*, Lecture Notes in Mathematics Vol. 1463 (Springer-Verlag, Berlin, 1991), pp. 65–79.  
 [17] H. Kidachi, Prog. Theor. Phys. **68**, 49 (1982).  
 [18] E. Knobloch and J. Guckenheimer, Phys. Rev. A **27**, 408 (1983).  
 [19] P. Hirschberg and E. Knobloch, J. Nonlinear Sci. **7**, 537 (1997).  
 [20] J. D. Crawford and E. Knobloch, Annu. Rev. Fluid Mech. **23**, 341 (1991).  
 [21] J. Knobloch and T. Wagenknecht, SIAM J. Appl. Dyn. Syst. **7**, 1397 (2008).  
 [22] J. Burke and E. Knobloch, Discrete Contin. Dyn. Syst. (to be published).  
 [23] J. R. Cash and D. R. Moore, BIT Numerical Mathematics **20**, 44 (1980).  
 [24] E. J. Doedel, A. R. Champneys, T. F. Fairgrieve, Y. A. Kuznetsov, B. Sandstede, and X.-J. Wang, Concordia University, 1997 (unpublished), available by FTP from ftp.cs.concordia.ca in directory pub/doedel/auto.  
 [25] M. Golubitsky and D. G. Schaeffer, *Singularities and Groups in Bifurcation Theory* (Springer, New York, 1984), Vol. 1.  
 [26] P. Assemat, A. Bergeon, and E. Knobloch, Phys. Fluids **19**, 104101 (2007).  
 [27] A. Bergeon, D. Henry, and E. Knobloch, Phys. Fluids **13**, 92 (2001).  
 [28] G. Kozyreff, P. Assemat, and S. J. Chapman (unpublished).  
 [29] K. Ghorayeb and A. Mojtabi, Phys. Fluids **9**, 2339 (1997).  
 [30] A. Bergeon and E. Knobloch, Phys. Fluids **20**, 034102 (2008).  
 [31] N. Tsitverblit and E. Kit, Phys. Fluids A **5**, 1062 (1993).  
 [32] N. Tsitverblit, Phys. Fluids **7**, 718 (1995).  
 [33] O. Batiste, E. Knobloch, A. Alonso, and I. Mercader, J. Fluid Mech. **560**, 149 (2006).